ARTICLE

Unpredicted Nucleation of Extended Zinc Blende Phases in Wurtzite ZnO Nanotetrapod Arms

Laura Lazzarini,[†] Giancarlo Salviati,[†,*] Filippo Fabbri,[†] Mingzheng Zha,[†] Davide Calestani,[†] Andrea Zappettini,[†] Takashi Sekiguchi,[‡] and Benjamin Dierre[‡]

[†]CNR-IMEM, University Campus, Viale G.P. Usberti 37/A, 43100 Parma, Italy, and [‡]Advanced Electronic Materials Center, National Institute of Materials Science, Tsukuba, Ibaraki 3050044, Japan

ABSTRACT Tailoring the structural and electronic properties of 3D nanostructures *via* bottom-up techniques would pave the way for novel low-cost applications. One of such possibilities is offered by ZnO branched nanostructures like tetrapods, that have recently attracted attention for nanodevice applications from nanoelectronics to drug delivery. The conventional picture is that ZnO arms are thermodynamically stable only in the wurtzite phase. Here, we provide the first experimental evidence of unpredicted extended zinc blend phases (50−60 nm long) embedded in the arms of ZnO wurtzite tetrapods. In particular, decisive evidence is obtained from the one-to-one correlation between high lateral resolution cathodoluminescence spectroscopy, monochromatic contrast maps, and atomic resolution transmission electron microscopy images of ZnO single TPs. This observation is not specific to ZnO and can have a general validity for the understanding of the nucleation mechanisms in semiconducting 3D nanostructures for device applications.

KEYWORDS: zinc oxide · tetrapods · cubic phase · cathodoluminescence · HRTEM

ZnO is a direct band gap (exp ~3.3 eV) semiconductor[1] crystallizing in the wurtzite (WZ) structure; the zinc blende (ZB) structure, which differs from WZ at the third neighbor only, is not observed in nature since thermodynamically it is a metastable phase. Pressure induced phase transitions from WZ to ZB are however achieved (>9 GPa) in commercial polycrystalline ZnO with a pronounced hysterisis or, in some cases, with a portion of the cubic phase persisting during decompression.[2] ZnO branched nanostructures like tetrapods (TPs), which are normally grown by strongly nonadiabatic techniques, can present polytypism because of the presence of a common polar axis (the stacking direction) and of the similarity of the nonpolar facets containing the full stacking sequence.[3] This can be true also for a variety of semiconductor nanostructures that are at present extensively studied[4−6] as the basis for novel material and devices. It is therefore interesting to trap the cubic structure at ambient conditions.

The growth of WZ ZnO branched nanostructures containing the ZB phase, allows in principle to interface different crystallographic structures with distinct electronic properties. Both the ZnO zinc blende and wurtzite lattices are noncentrosymmetric and can thus sustain the piezoelectric effect; furthermore, the hexagonal structure (WZ) exhibits a unique rotation axis (the polar 6-fold axis) and is thus compatible with the conditions for pyroelectricity[7] and spontaneous polarization, which are absent in ZB. The two phases exhibit different band gaps, electronic and elastic properties. So, the presence of cubic and hexagonal phases in the same tetrapod offers novel routes in the design of nanodevices made by a single nanostructure. Indeed, the possibility to obtain alternating WZ and ZB phases along the TP arms, as already shown in III−V NWs where the ZB and WZ phases are both thermodynamically allowed,[8] would be extremely interesting and intriguing since the nanostructure spontaneously presents one arm oriented perpendicular to the substrate. This finding leaves the field open for fundamental research and device application allowing in principle to design nanodevices[9−15] or to electrodynamically confine a single ZnO TP, to manipulate its position, and to make it lasing[16] or to exploit a different response to surface functionalization. Up to now, in the literature, the ZB phase in ZnO TPs has been discussed only in relation to the nature of the TP core. Some models have been proposed to explain the nucleation of the WZ TP arms either on ZB[17,18] or WZ[19−21] cores. Recently, the nucleation of ZnO TPs with wurtzite-type arms branching off a zinc blend core[6,22] has been directly observed. An-

*Address correspondence to Giancarlo.Salviati@cnr.it, salviati@imem.cnr.it.

Received for review May 28, 2009 and accepted August 26, 2009.

Published online September 9, 2009. 10.1021/nn900558q CCC: $40.75

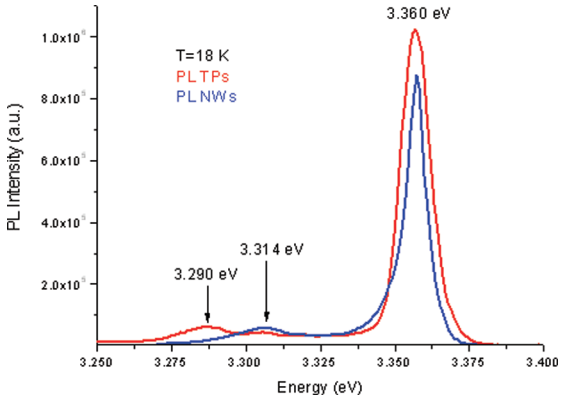

Figure 1. Large area PL spectra of a bunch of hundreds of TPs (red curve) and NWs (blue curve). The usual behavior of an NBE transition as a function of decreasing temperature has been verified.

other group[23] grew single-crystal ZnO cubic nanorods on patterned substrates.

To our knowledge, concerning the ZnO TPs, all the researchers however agree that the arms have a WZ structure. Here we report on the first experimental evidence of *large portions* (50−60 nm in length and as large and thick as the whole arms) of zinc blende phase found *embedded* in the arms as well as at the arm tips in catalyst-free TPs nucleating as a floating particulate brought by a gas stream (see Experimental Methods). Employing high lateral resolution cathodoluminescence (CL) spectroscopy and monochromatic imaging, high resolution transmission electron microscopy (HRTEM) and photoluminescence (PL) spectroscopy, we provide a detailed study of the TP arms and characterize the heteropolytype structure: the complete correspondence between the ZB CL imaging and HRTEM analyses confirms this result, by providing a direct image of the different zones. No evidence of the ZB phase in all the other WZ ZnO nanostructures (nanocombs, nanowires) grown with the same technique under different growth conditions has been found. Our findings of the cubic phase at the TP arms and tips contradict the conclusions based on thermodynamic reasons that the ZB cannot grow upon the WZ phase.

RESULTS AND DISCUSSION

The optical properties of bunches of TPs have been studied by large area PL spectroscopy at liquid helium temperature and the results have been compared with those obtained from ZnO nanowires (NWs) and nanocombs (NCs). The comparison (Figure 1), revealed that only the TPs presented a typical emission peak at 3.29 eV. Since the dimensions of our TPs do not allow for any quantum confinement effects, the interpretation of the spectra has been done on the basis of literature data concerning bulk ZnO emissions. As a consequence, the band at 3.29 eV has been attributed to the ZB ZnO near band edge (NBE) emission at 10 K.[24] In addition, the band peaks at 3.36 eV and at 3.314 eV have been ascribed to the NBE[3] and to the exciton to neutral acceptor (A^0X)[25] transitions in WZ ZnO, respectively.

To precisely determine the relative spatial distribution of the WZ and ZB phases inside the TPs and to study the influence of the growth parameters on both the onset and spatial localization of the ZB phase, CL spectroscopy and monochromatic imaging at liquid Helium temperature have been carried out on single TPs with variable dimensions and shape.

Figure 2a shows a typical CL spectrum of the TP reported in Figure 2b. Accurate Gaussian multipeak deconvolution procedures gave the main peak centered at 3.36 eV due to four bands. The first one at 3.373 eV is assigned to the WZ ZnO free exciton (FX) emission[26] and the remaining ones at 3.363, 3.354, and 3.352 eV are assigned to bound exciton to neutral donor transitions (D^0X).[26] Furthermore, the peaks at 3.308 and 3.314 eV are found to be due to WZ exciton-to neutral acceptor (A^0X)[25] or the first LO phonon replica of the WZ phase[26] and free electron to neutral acceptor (A^0e) transitions with the acceptor states confined to basal stacking faults (SFs), respectively.[27]

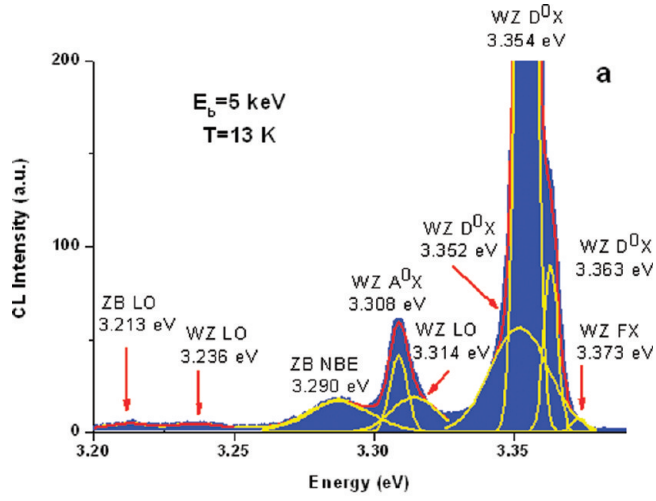

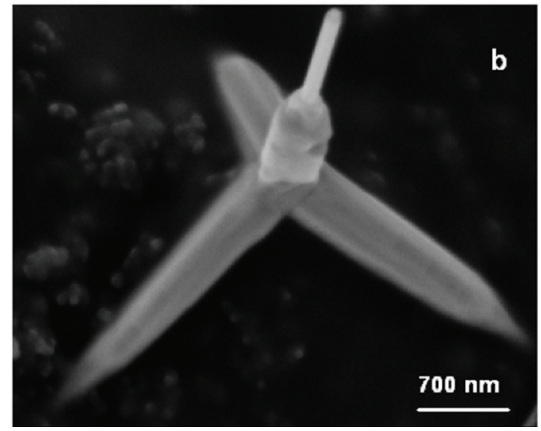

Figure 2. (a) Experimental CL spectrum of the micrometric ZnO TP reported in panel b. T = 13 K, beam energy E_b= 5 keV. (b) Typical TP collected from the high temperature zone of the reactor (T = 650 °C). The average arm length is more than 1 μm. The gray features on the background come from the carbon tape used to stick the TP.

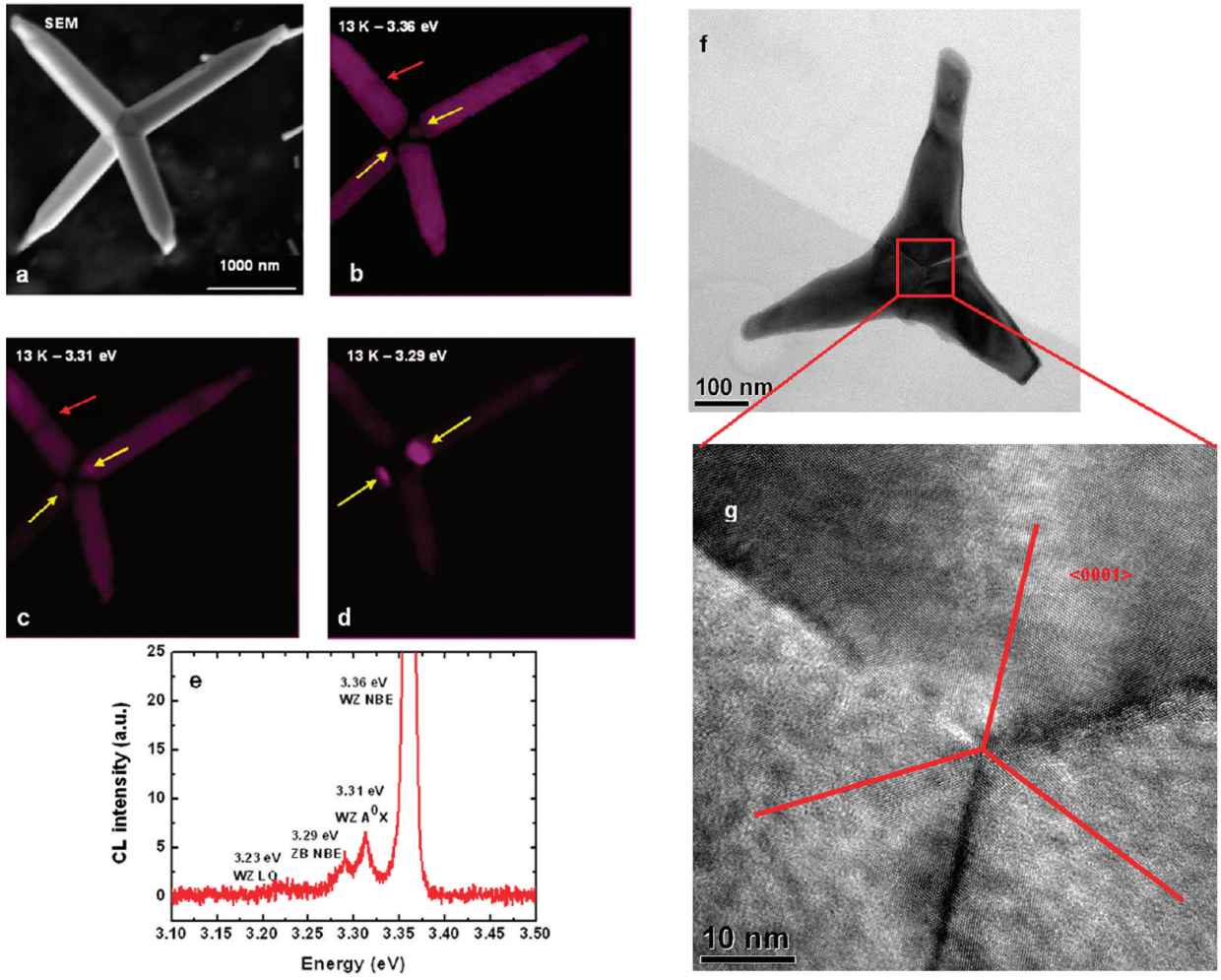

Figure 3. Comparison among the secondary electron (SE) (a) and low temperature monochromatic CL images in false colors (panels b, c, and d taken at the NBE energy values of WZ (3.36 eV), WZ A^0X (3.31 eV), and ZB (3.29 eV) phases, respectively. The cubic emission in panel d comes from SFs located at the TP interface between core and legs. Panel e reports the CL spectrum from the TP in panel a obtained at $T = 13$ K. The TP has been collected from the high temperature zone of the reactor ($T = 650$ °C). (f) Zero loss filtered TEM image of a typical small TP; the fourth leg is hidden and visible as a dark shadow in the center. (g) HRTEM picture of the TP from the red square in panel f showing the legs are WZ type, with the growth directions along the *c*-axis and arranged according to the hexagonal symmetry (angles in among each other are about 120°).

As for the band at 3.29 eV, by comparing our CL spectroscopy and imaging and HRTEM structural investigations (see discussion on Figures 1−4) and in agreement with recent works,[24,28,29] we can unambiguously state that the band at 3.29 eV arises from the ZB NBE emission. Following,[25,30] the 3.236 and 3.213 eV transitions can be due to WZ and ZB LO phonon replicas, respectively. It is worth noting that the difference between the center of mass of the WZ and ZB NBE peaks (~64 meV) is in fairly good agreement with density functional theory (DFT) results[31] and only slightly smaller than the value of 80 meV reported by Yeh *et al.*[32]

Figure 3 shows typical monochromatic images of the spatial distribution of WZ and ZB emissions from a single tetrapod of micrometer scaled dimensions. Figure 3a shows the conventional SEM image of the specific tetrapod studied. In Figure 3b the spatial distribution of the NBE emission of the WZ phase obtained collecting the sole emission at 3.36 eV (monochromatic CL imaging) is shown. It is apparent that the CL emission from the hexagonal phase is homogeneously distributed all across the TP arms except for the presence of triangular-shaped nonradiative recombination lines (marked with yellow arrows) at the interface between the TP core and the protruding arms. An additional fainter dark line can be also seen along one of the arms (red arrow). Accurate HRTEM studies of the core structure of hundreds of TPs with variable dimensions revealed the presence of basal-plane SFs and/or twin boundaries (TBs) in all the samples investigated. Thus observation drives us to ascribe the CL nonradiative lines arranged in a triangular shape in Figure 2b to the presence of SFs at the boundaries between the arms (WZ/WZ interface with a twin relationship[22]) or between the arms

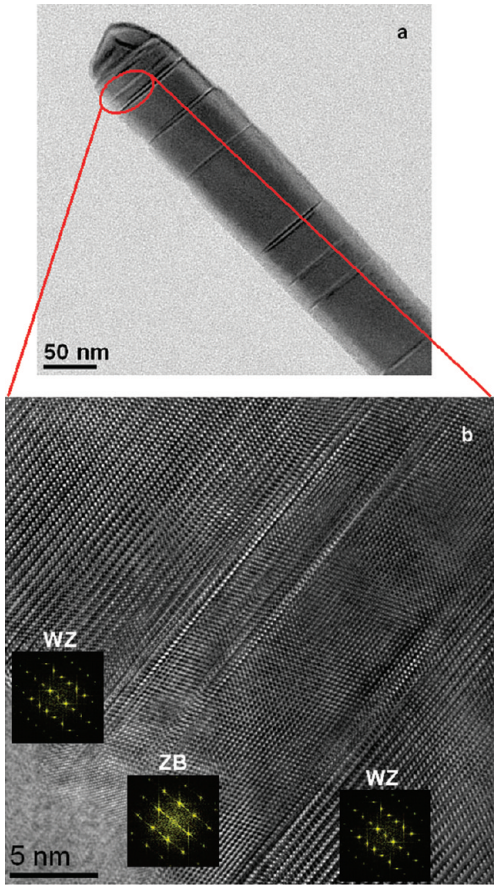

Figure 4. (a) Zero loss low magnification TEM image of a TP arm obtained under optimum diffraction contrast conditions to show a sequence of SFs, $\mathbf{g} = \langle 0001 \rangle$ type; (b) BF HRTEM micrograph of the elliptical portion in red shown in panel a. The sequence of extended WZ/ZB/WZ areas is shown by the diffractograms reported as insets.

and the core (WZ/WZ or possibly ZB/WZ interface)[33] and/or to twin boundaries.[21,33,34]

The micrographs in Figure 3 panels c and d are taken by collecting and imaging only the CL emissions at 3.31 and 3.29 eV, respectively (see Figure 3e). Note the spatial localization of those emissions at the interface between TP core and legs. It is worth mentioning that two of the nonradiative recombination lines at 3.36 eV, indicated by yellow arrows, become bright when the CL monochromatic emission at 3.31 eV is collected. This result suggests a strong asymmetric segregation of intrinsic point defects (*e.g.*, V_{Zn}, O_i, O_{Zn})[27] between the four legs of the TPs, due to the strain field at planar defects, resulting in a transition involving a shallow acceptor. The reason of the asymmetry could be correlated to different internal strain fields, to different planar defect reactivity (SFs, TBs) or to different polarization fields. Furthermore, the assignment of the transition to native point defects also explains the homogeneous distribution of the luminescence all along the TP arms. Finally, the presence of a cubic phase at the basis of the protruding arm is also apparent (Figure 3d, −3.29 eV). Following the CL results, HRTEM has been used to study first the crystal structure of the TP cores. Contrary to what was expected from previous results,[22] it is worth noting that all the TPs investigated, independently on the leg dimensions, did not reveal any extended portions of cubic symmetry at the TP cores (Figure 3f,g). Our branched nanostructures nucleate from an hexagonal core following the model proposed in the literature;[19−21] as a consequence, the CL monochromatic imaging of a cubic phase inside the TP cores must be ascribed to the nucleation of SFs[17,19,22] and/or TBs,[21,33,34] in agreement with the structural results that consider the formation of basal-plane stacking faults at the leg/core interfaces as the driving force for the nucleation of the WZ phase onto a ZB one.[35,36]

The reason of the strong localization of the CL cubic emission at the SFs is that the WZ/ZB interface exhibits a type-II line-up (see ref 35 for ZnO and ref 37 for III-nitrides). The SFs induce a downward shift of the conduction band minimum (CBM), they have a direct band gap at Γ and act as quantum well-like structures for electrons and holes. However, the SFs are not supposed to induce any quantum confinement since the CBM states are not to be found very localized.[35] However, since a deeper discussion of the TP cores is beyond the purpose of this paper, in the following we will focus on the optical and structural properties of only the TP arms.

Accurate CL and HRTEM investigations of TPs with an average dimension similar to those shown in Figure 2 and Figure 3 did not reveal ZB extended phases along the arms, only SFs and TBs have been found. When TPs

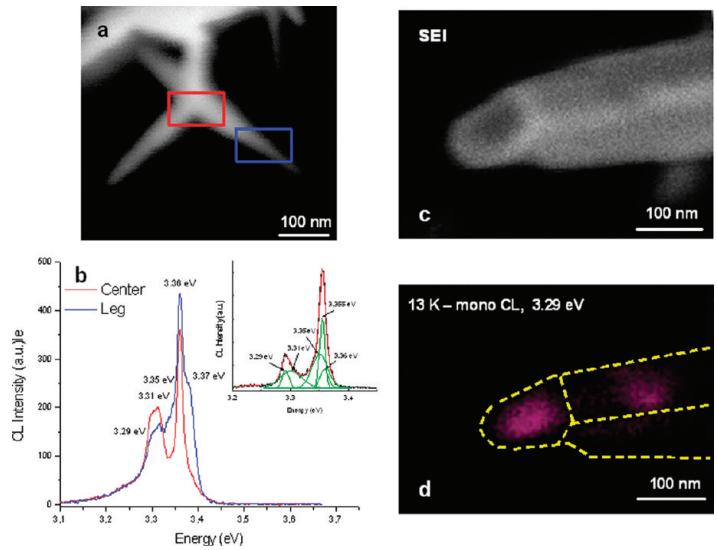

Figure 5. (a) SEM micrograph of a nanometer sized TP; (b) the blue and red CL spectra have been collected from the blue and red rectangular areas in panel a. The inset represents the CL spectrum from the whole TP. Gaussian deconvolution procedures gave the usual WZ and ZB energy values. The CL spectra have been acquired at a beam energy $E_b = 5$ kV, $T = 10$ K and 500 000 times of magnification. For that reason the spectra are slightly noisy. (c) SEM picture of a portion of a TP arm of about 500 nm in length; (d) false color monochromatic CL image of the same area as in panel c. The emission from the ZB phase (3.29 eV) at the arm tip and from an intermediate zone is shown.

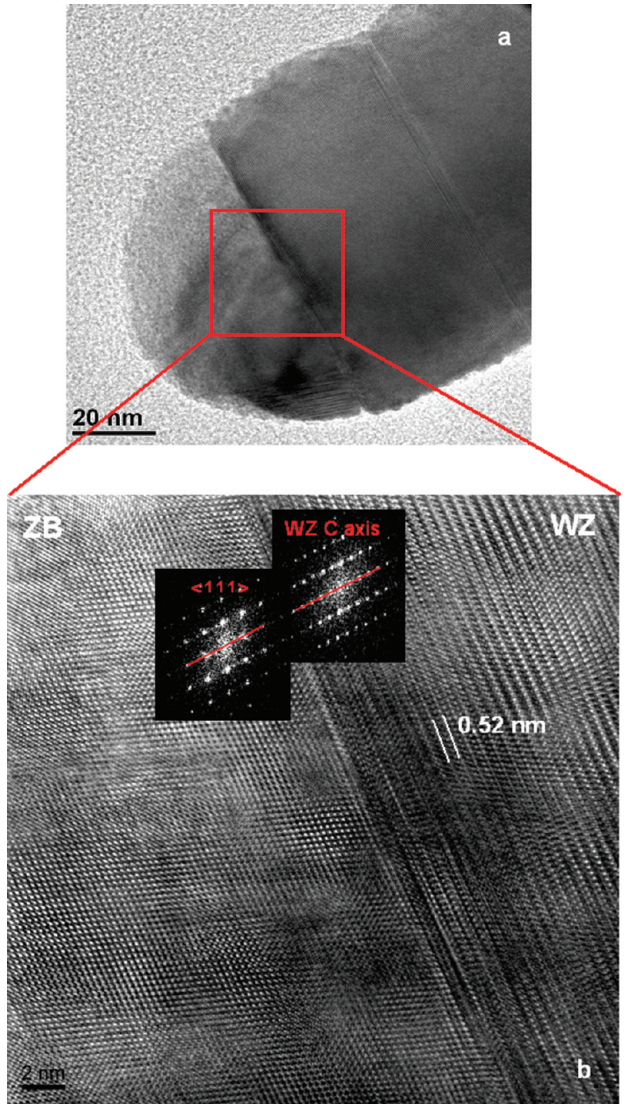

Figure 6. (a) Atomic resolution TEM micrograph of an arm tip of a TP collected in the coldest area of the reactor (200 °C < *T* < 415 °C). The extended ZB phase (40 nm × 80 nm) nucleates onto a WZ area; a basal SF is also shown at the WZ/ZB interface; (b) enlargement of a portion of the cubic/hexagonal interface area (red square). Cubic and hexagonal diffractograms from the tip and arm are respectively reported in the insets showing the parallelism between the WZ C axis and the ⟨111⟩ type directions of the ZB lattice (the red lines are guides for the eyes).

collected from areas of the reactor at lower temperatures (smaller average size) are investigated, a different scenario comes out and in addition to SFs, HRTEM investigations of the sample arms surprisingly *reveal the unexpected and unpredicted presence of extended cubic phases in between hexagonal ones* (Figure 4a,b). TPs with arms shorter than 200−300 nm in length are then fully investigated. Figure 5 panels a and b show the SEM images of a TP with arms shorter than 200 nm and the LT CL spectra from the core and one tip, respectively. In this case, the presence of cubic phase emission also at the TP tip is found as shown by accurate Gaussian deconvolution reported in the inset of Figure 5b. In some cases it has been possible to image the monochromatic CL emission from the cubic phase along the arm as shown in Figure 5d. Note that the lateral dimension of the CL emission contrast from the ZB areas is larger than the size of the cubic phases in HRTEM images (see Figures 4 and 6) because of the influence of the experimental parameters on the lateral resolution of the CL technique.[38] Also in this case, HRTEM studies reveal extended cubic phases at the TP arm tips with an even larger dimension. As an example, Figure 6 shows wide ZB zones at the tip of the TP (40−50 nm along the growth axis) collected from an oven area at 200 °C < *T* < 415 °C. It is worth noting that the lateral dimension of these cubic phases is much larger than that of the SFs that do not extend more than a few atomic layers.[35,39] Our results, in contradiction to theoretical calculations,[32,40] demonstrate that the nucleation of stable, extended, and alternating ZB/WZ phases (see Figures 4b and 6b) is allowed under suitable growth conditions along ZnO TP arms.

The growth method used for obtaining our TPs is a catalyst-free "*in-stream*" mechanism which can allow us to control and modulate the shape of ZnO TPs[41] and presents different growth conditions from those employed to grow our ZnO nanocombs, nanowires, *etc*. As for our experiments, while NCs and NWs grow in Zn excess conditions onto a substrate where liquid Zn droplets are present, the TPs directly nucleate while floating in the vapor phase at very high Zn and O supersaturation conditions, that is, out of the thermodynamic equilibrium conditions (see Experimental Methods). Further theoretical studies must be carried out to develop a quantitative model to explain the existence of an extended cubic phase at the tip of the TP arms. However, the main purpose of this paper was to give a solid experimental evidence of the occurrence of ZB stable and extended phases at the TP arms and the achievement of a growth procedure to obtain nano TPs with coexisting WZ and ZB phases. We believe our results have a general validity for semiconduting nanostructures and we expect they will stimulate new contributions from theoreticians and experts in principles of crystal growth. It is in fact well-known that, in addition to ZnO, the ZB phase is the initial nucleus also for the growth of nanostructures like ZnS, CdSe, CdS, and MnS[42−46] even if it is rather unstable and quickly transforms into the WZ phase as the crystal becomes bigger.

In conclusion, the nucleation of cubic ZnO massive phases embedded into the hexagonal arms of nanotetrapods has been experimentally shown. Different ZnO nanostructures, like nanowires or nanocombs, do not present any ZB phases. This observation has been ascribed to the different growth conditions used. The structural and optical properties of single tetrapods have been studied by HRTEM and SEM-CL spectroscopy and imaging. The results showed a one-to-one spatial correspondence between the monochromatic CL imaging of the ZB phase NBE emission and HRTEM lattice micrographs. The cubic zones have been found in nanometer-sized TPs, mean-

while, in micrometer-sized TPs, there is no evidence of cubic phase embedded into the arms of the nanostructures. The influence of the temperature gradient and Zn and O supersaturation conditions inside the reactor has been qualitatively correlated to the onset of alternating bulk ZB/WZ phases inside the arms of the smallest tetrapods.

EXPERIMENTAL METHODS

"In-Stream" Vapor Phase Growth of the ZnO TPs. The growth method used for obtaining our TPs is a catalyst-free vapor-solid mechanism.[41] In particular ZnO tetrapods have been grown by a combination of thermal evaporation and controlled oxidation. The growth process was performed in a tubular furnace, where different gases can be introduced through proper flow-controllers. Pure metallic Zn (6 N) foils were used as source material and no other catalyst, precursor, or potential contaminant were added. Source material was heated up to 650 °C in an inert gas (Ar) flow (20 sccm) and, when this temperature was reached, Ar flow was substituted by an Ar/O_2 mixture (20:1 ratio, 100 sccm), thus starting the formation of a light white "smoke" in the reaction tube. The floating white particulate was made of tetrapods and it was brought by the gas stream up to the colder zone of the reactor, where it deposited on the tube walls.

The TP nucleation and size are determined by the Zn/O ratio in the vapor and by the local temperature in the reactor. Generally the larger TPs (micrometer-sized) grow at higher temperatures and Zn vapor concentration; opposite conditions lead to a reduced nucleation/growth rate, that is, to smaller TPs (nanometer sized). The arms of these nanostructures grow while TPs are being transported by the inert gas flow, together with vapor phase reagents (Zn and O_2), toward the colder zone of the reactor. In this zone the growth ends and TPs settle on the tube walls. During their "growth path" along the reactor, the TPs can experience different local conditions (Zn/O ratio, temperature, *etc.*): the terminal ZB phase can be found only for small-sized TPs grown at low temperature, with low Zn/O flux, that is, with poor mobility of the elemental species, indicating the existence of a possible critical dimension above which ZB cannot be further stabilized.

Optical Characterization. The morphology and size of "as-grown" single ZnO tetrapods as well as cathodoluminescence (CL) spectroscopy and monochromatic imaging were performed by using a field emission scanning electron microscope (Hitachi S4200) equipped with a CL system.[47] To this purpose, the nanostructures were removed from their substrate and dispersed on conductive carbon tape. CL investigations were performed by using primary electron beam energy/current values of 5 keV/0.2 nA at 10 K.

Photoluminescence (PL) measurements were taken using the 325 nm line of a He−Cd laser as an excitation source. The sample was mounted in a cryostat where the temperature can be varied in the range 14−300 K.

Transmission Electron Microscopy Studies. For TEM studies, the TPs were first sonicated from the growth substrate and then dispersed onto Cu/lacey-carbon TEM grids. A field emission high resolution (Scherzer resolution = 0.19 nm) analytical TEM working at 200 kV (JEOL JEM-2200 FS) has been used to study the structural properties of single TPs. As for the determination of the crystallographic phases, hundreds of TPs of variable sizes have been analyzed to achieve reliable statistics for the observations.

Acknowledgment. This work has been partly supported by the Significant Project of the Italian Ministry of Foreign Affairs "Nanocharacterization of Nanowires, Nanomagnets and laser diodes for sensors, optoelectronics and data storage (N3)".

REFERENCES AND NOTES

1. Wang, Z. L.; Kong, X. Y.; Ding, Y.; Gao, P.; Huges, W. L.; Yang, R.; Zhang, Y. Semiconducting and Piezoelectric Oxide Nanostructures Induced by Polar Surface. *Adv. Funct. Mater.* **2004**, *14*, 843–956.
2. Boulfelfel, S. E.; Leoni, S. Competing Intermediates in the Pressure-Induced Wurtzite to Rocksalt Phase Transition in ZnO. *Phys. Rev. B* **2008**, *78*, 125204–125207.
3. Newton, M. C.; Warburton, P. A. ZnO Tetrapod Nanocrystals. *Mater. Today* **2007**, *10*, 50–54.
4. Xie, R.; Kolb, U.; Basch, T. Design and Synthesis of Colloidal Nanocrystal Heterostructures with Tetrapod Morphology. *Small* **2006**, *2*, 1454–1457.
5. Manna, L.; Milliron, D. J.; Meisel, A.; Scher, E. C.; Alivisatos, P. Controlled Growth of Tetrapod-Branched Inorganic Nanocrystals. *Nat. Mater.* **2003**, *2*, 382–385.
6. Yoo, Y.-Z.; Osaka, Y.; Fukumura, T.; Jin, Z.; Kawasaki, M.; Koinuma, H. High Temperature Growth of ZnS Films on Bare Si and Transformation of ZnS to ZnO by Thermal Oxidation. *Appl. Phys. Lett.* **2001**, *78*, 616–618.
7. Nye, J. *Physical Properties of Crystals*, Oxford University Press, London, 1957.
8. Caroff, P.; Dick, K. A.; Johansson, J.; Messing, M. E.; Deppert, K.; Samuelson, L. Controlled Polytypic and Twin-Plane Superlattices in III−V Nanowires. *Nat. Nanotechnol.* **2009**, *4*, 50–55.
9. Stichtenoth, D. C.; Ronning, C.; Niermann, T.; Wischmeier, L.; Voss, T.; Chien, C. J.; Chang, P. C.; Lu, J. G. Optical Size Effects in Ultrathin ZnO Nanowires. *Nanotechnology* **2007**, *18*, 435701–435705.
10. Huang, M.; Mao, S.; Feick, H.; Yan, H.; Wu, Y.; Kind, H.; Weber, E.; Russo, R.; Yang, P. Room-Temperature Ultraviolet Nanowire Nanolaser. *Science* **2001**, *292*, 1897–1899.
11. Liu, C.; Zapien, J. A.; Yuan, Y.; Xiangmin, M.; Chun, S. L.; Shoushan, F.; Lifshitz, Y.; Shuit, T. L. High-Density, Ordered Ultraviolet Light-Emitting ZnO Nanowire Arrays. *Adv. Mater.* **2003**, *15*, 838–841.
12. Sun, B. Q.; Marx, E.; Greenham, N. C. Photovoltaic Devices Using Blends of Branched CdSe Nanoparticles and Conjugated Polymers. *Nano Lett.* **2003**, *3*, 961–963.
13. Wang, Z.; Kong, X. Y.; Zuo, J. M. Induced Growth of Asymmetric Nanocantilever Arrays on Polar Surfaces. *Phys. Rev. Lett.* **2003**, *91*, 185502–185505.
14. Wang, X.; Summers, C. J.; Wang, Z. L. Large-Scale Hexagonal-Patterned Growth of Aligned ZnO Nanorods for Nano-Optoelectronics and Nanosensor Arrays. *Nano Lett.* **2004**, *4*, 423–426.
15. Pellegrino, T.; Kudera, S.; Liedl, T.; Muñoz Javier, A.; Manna, L.; Parak, W. J. On the Development of Colloidal Nanoparticles towards Multifunctional Structures and their Possible Use for Biological Applications. *Small* **2005**, *1*, 48–63.
16. Mondia, J. P.; Sharma, R.; Schäfer, J.; Smith, W.; Zhao, Y. P.; Lu, Z. H.; Wang, L. J. An Electrodynamically Confined Single ZnO Tetrapod Laser. *Appl. Phys. Lett.* **2008**, *93*, 121102.
17. Shiojiri, M.; Kaito, C. Structure and Growth of ZnO Smoke Particles Prepared by Gas Evaporation Technique. *J. Cryst. Growth* **1981**, *52*, 173–177.
18. Nishio, K.; Isshiki, T.; Kitano, M.; Shiojiri, M. Structure and Growth Mechanism of Tetrapod-like ZnO Particles. *Philos. Mag., A* **1997**, *76*, 889–904.
19. Fujii, M.; Iwanaga, H.; Ichihara, M.; Takeuchi, S. Structure of Tetrapod-like ZnO Crystals. *J. Cryst. Growth* **1993**, *128*, 1095–1098.
20. Ronning, C.; Shang, N. G.; Gerhards, I.; Hofsäss, H.; Seibt, M. Nucleation Mechanism of the Seed of Tetrapod ZnO Nanostructures. *J. Appl. Phys.* **2005**, *98*, 034307.
21. Liu, Z.; Zhang, X.; Hark, S. K. Quadra-Twin Model for Growth of Nanotetrapods and Related Nanostructures. *J. Phys. Chem. C* **2008**, *112*, 8912–8916.
22. Ding, Y.; Wang, Z. L.; Sun, T.; Qiu, J. Zinc-Blende ZnO and its Role in Nucleating Wurtzite Tetrapods and Twinned Nanowires. *Appl. Phys. Lett.* **2007**, *90*, 153510.

23. Zhou, S. M.; Gong, H. C.; Zhang, B.; Du, Z. L.; Zhang, X. T.; Wu, S. X. Synthesis and Photoluminescence of a Full Zinc Blende Phase ZnO Nanorod Array. *Nanotechnology* **2008**, *19*, 175303–175306.
24. Kim, S. K.; Jeong, S. Y.; Cho, C. R. Structural Reconstruction of Hexagonal to Cubic ZnO Films on Pt/Ti/SiO_2/Si Substrate by Annealing. *Appl. Phys. Lett.* **2003**, *82*, 562–564.
25. Klingshirn, C. ZnO: From Basics towards Application. *Phys. Status Solidi B* **2007**, *244*, 3027–3073.
26. Klingshirn, C. ZnO: Material, Physics and Applications. *Chem Phys Chem* **2007**, *8*, 782–803.
27. Schirra, M.; Schneider, R.; Reiser, A.; Prinz, G. M.; Feneberg, M.; Biskupek, J.; Kaiser, U.; Krill, C. E.; Sauer, R.; Thonke, K. Acceptor-Related Luminescence at 3.314 eV in Zinc Oxide Confined to Crystallographic Line Defects. *Phys. B* **2007**, *401*−*402*, 362–365.
28. Özgür, Ü.; Alivov, Ya. I.; Liu, C.; Teke, A.; Reshchikov, M. A.; Dogan, S.; Avrutin, V.; Cho, S. J.; Morkoç, H. A Comprehensive Review of ZnO Materials and Devices. *J. Appl. Phys.* **2005**, *98*, 041301.
29. Lee, C. H.; Kawazoe, T.; Ohtsu, M. The Difference in Optical Bandgap between Zinc Blend and Wurtzite ZnO Structure Formed on Sapphire (0001) Substrate. *Solid State Commun.* **2003**, *124*, 163–165.
30. Gruzintsev, N. A.; Red'kin, A. N.; Makovei, Z. I.; Kozlovskii, V. I.; Skasyrskii, Ya. K. Luminescent Properties of Vertically Aligned ZnO Nanorod Arrays Grown on (100) Si Substrates. *Inorg. Mater.* **2006**, *42*, 872–876.
31. Janotti, A.; Segev, D.; Van de Walle, C. G. Effects of Cation d States on the Structural and Electronic Properties of III-Nitride and II-Oxide Wide-Band-Gap Semiconductors. *Phys. Rev. B* **2006**, *74*, 045202−045210 and references therein.
32. Yeh, C.; Wei, S.; Zunger, A. Relationships between the Band Gaps of the Zinc-Blende and Wurtzite Modifications of Semiconductors. *Phys. Rev. B* **1994**, *50*, 2715–2718.
33. Wang, B. B.; Ji-Jia; Xie, J. J.; Yuan, Q.; Zhao, Y. P. Growth Mechanism and Joint Structure of ZnO Tetrapods. *J Phys D: Appl. Phys.* **2008**, *41*, 102005–102010.
34. Yan, Y.; Al-Jassim, M. M.; Chisholm, M. F.; Boatner, L. A.; Pennycook, S. J.; Oxley, M. [11 00] /(1102) Twin Boundaries in Wurtzite ZnO and Group-III-Nitrides. *Phys. Rev. B* **2005**, *71*, 041309−041312(R).
35. Yan, Y.; Dalpian, G. M.; Al-Jassim, M. M.; Wei, S. H. Energetics and Electronic Structure of Stacking Faults in ZnO. *Phys. Rev. B* **2004**, *70*, 193206–193209.
36. Ashrafi, A.; Jagadish, C. Review of Zincblende ZnO: Stability of Metastable ZnO Phases. *J. Appl. Phys.* **2007**, *102*, 071101.
37. Salviati, G.; Albrecht, M.; Zanotti-Fregonara, C.; Armani, N.; Mayer, M.; Shreter, Y.; Guzzi, M.; Melnik, Y. V.; Vassilevski, K.; Dmitriev, V. A.; Strunk, H. P. Cathodoluminescence and Transmission Electron Microscopy Study of the Influence of Crystal Defects on Optical Transitions in GaN. *Phys. Status Solidi A* **1999**, *171*, 325–339.
38. Salviati, G.; Armani, N.; Rossi, F.; Lazzarini, L.; Grillo, V. Power Dependent Cathodoluminescence in III−V Nitrides Heterostructures: From Internal Field Screening to Controlled Band Gap Modulation. In *Characterization of Semiconductor Heterostructures and Nanostructures*; Lamberti, C., Ed.; Elsevier: New York, 2008, 209−248.
39. Thonke, K.; Schirra, M.; Schneider, R.; Reiser, A.; Prinz, G. M.; Feneberg, M.; Biskupek, J.; Kaiser, U.; Sauer, R. The Role of Stacking Faults and their Associated 0.13 eV Acceptor State in Doped and Undoped ZnO Layers and Nanostructures. *Microelectron. J.* **2009**, *40*, 210–214.
40. Serrano, J.; Romero, A. H.; Manjon, F. J.; Lauck, R.; Cardona, M.; Rubio, A. Pressure Dependence of the Lattice Dynamics of ZnO: An *ab initio* Approach. *Phys. Rev. B* **2004**, *69*, 094306−094319.
41. Qiu, Y.; Yang, S. ZnO Nanotetrapods: Controlled Vapor-Phase Synthesis and Application for Humidity Sensing. *Adv. Funct Mater.* **2007**, *17*, 1345–1352.
42. Jun, Y. W.; Jung, Y. Y.; Cheon, J. Architectural Control of Magnetic Semiconductor Nanocrystals. *J. Am. Chem. Soc.* **2002**, *124*, 615–619.
43. Milliron, D. J.; Huges, S. M.; Cui, Y.; Manna, L.; Li, J.; Wang, L. W.; Allivisatos, A. P. Colloidal Nanocrystal Heterostructures with Linear and Branched Topology. *Nature* **2004**, *430*, 190–195.
44. Chen, M.; Xie, Y.; Lu, J.; Xiong, Y.; Zhang, S.; Qian, Y.; Liu, X. Synthesis of Rod-, Twinrod-, and Tetrapod-Shaped CdS Nanocrystals Using a Highly Oriented Solvothermal Recrystallization Technique. *J. Mater. Chem.* **2002**, *12*, 748–753.
45. Gong, J.; Yang, S.; Huang, H.; Duan, J.; Liu, H.; Zhao, X.; Zhang, R.; Du, Y. Experimental Evidence of an Octahedron Nucleus in ZnS Tetrapods. *Small* **2006**, *2*, 732–735.
46. Pang, Q.; Zhao, L.; Cai, Y.; Nguyen, D. P.; Regnault, N.; Wang, N.; Yang, S.; Ge, W.; Ferreria, R.; Bastard, G.; Wang, J. CdSe Nano-Tetrapods: Controllable Synthesis, Structure Analysis, and Electronic and Optical Properties. *Chem. Mater.* **2005**, *17*, 5263–5267.
47. Sekiguchi, T. Development of Low Energy Cathodoluminescence System and its Application to the Study of ZnO Powders. *Mater. Res. Soc. Symp. Proc.* **2000**, *588*, 75–80.